Chinese Chemical Letters 35 (2024) 108595

Contents lists available at ScienceDirect

Chinese Chemical Letters

journal homepage: www.elsevier.com/locate/cclet

Synthesis of photostable near-infrared sulfone-rhodamines for photoacoustic imaging-guided photothermal therapy

Huiyu Si[a], Dongjuan Wang[a], Xianfa Du[b], Xin Zhou[a,*]

[a] Department of Chemistry, College of Chemistry and Chemical Engineering, Qingdao University, Qingdao 266071, China
[b] Department of Orthopedics, the Affiliated Hospital of Qingdao University, Qingdao 266071, China

ARTICLE INFO

Article history:
Received 2 April 2023
Revised 18 May 2023
Accepted 19 May 2023
Available online 24 May 2023

Keywords:
Photothermal therapy
Sulfone rhodamine
Near-Infrared
Photoacoustic
Imaging

ABSTRACT

Photothermal therapy (PTT) is a cutting-edge cancer treatment that can kill cancer cells in hypoxic environments without relying on oxygen. Seeking of the ideal photothermal agents with a high absorption coefficient in the near-infrared region, and a high excellent photothermal conversion efficiency is of great significance. Sulfone-Rhodanmine dye has showed an impressive absorption wavelength over 700 nm, but suffered from a stability issue. In this study, we synthesized five sulfone rhodamines and investigated the substitution effects on stability. **SO_2R2** showed high stability and strong absorbance at 714 nm with an excellent photothermal conversion efficiency of 53.06%, making it suitable for accurate photoacoustic imaging-guided photothermal therapy *in vivo*.

Photothermal therapy (PTT) is a cutting-edge cancer treatment that uses high-efficiency photothermal conversion materials to convert light energy into heat energy, effectively killing cancer cells with near-infrared light [1–8]. PTT is unique because it can kill cancer cells in hypoxic environments without relying on oxygen [9–13]. When the photothermal agent absorbs energy, it generates heat that kills cancer cells and produces photoacoustic (PA) signals, enhancing its diagnostic capabilities [14–21].

Recently, continuous work has been focused on developing photothermal conversion agents to discover the more effective phototherapy treatment [22,23]. Generally, the ideal photothermal agents must have a high absorption coefficient in the near-infrared region, and a high excellent photothermal conversion efficiency, as well as excellent biocompatibility [24–28]. The excellent properties of fluorescent dyes have promoted the progress of bioimaging technology [29,30]. Among them, rhodamine dyes have received great attentions due to their advantages, such as large molar absorbance coefficient, high fluorescence quantum yield, excellent lightfastness, and adjustable excitation and emission wavelengths [31,32]. Moreover, it has been demonstrated that modifying the rhodamine core with heteroatoms can redshift their absorbance and emissions [33,34]. For example, substitution with sulfone can achieve an impressive absorption wavelength around 700 nm, making it an excellent candidate for biological imaging and phototherapy [35,36]. However, such an electron-withdrawing sulfone group can cause the C-9 position of the rhodamine core to become more susceptible to nucleophiles, such as water and thiols, resulting in instability and rendering them unsuitable for further biological applications. Therefore, developing high-stability sulfone rhodamine dyes is in high demand.

In this study, we synthesized five sulfone rhodamines and investigated the substitution effects on their stability. As shown in Fig. 1, the ortho-substituent is crucial for protecting the C-9 site from nucleophilic attack. Among them, **SO_2R2**, which contains a CF_3 group, showed high stability and strong absorbance at 714 nm. *In vitro* studies revealed that this compound exhibited excellent photothermal conversion efficiency of 53.06% and good biocompatibility, making it a promising therapeutic diagnostic agent. Furthermore, *in vivo* studies confirmed that **SO_2R2** produced a robust photoacoustic signal (PA) and achieved local heating upon laser irradiation, leading to inhibition of tumor growth without significant side effects.

As depicted in Fig. S2A (Supporting information), all compounds exhibited absorption peaks around 700 nm in water solution. The emission spectrum of **SO_2R1**–**SO_2R5** were measured in CH_2Cl_2, CH_3CN and H_2O. The emission peaks of **SO_2R1**–**SO_2R5** were centered around 730 nm. We determined their fluorescence quantum yields (Φ_f) by taking Rhodamine B as the control [37]. As shown in Fig. S3 (Supporting information), all dyes showed high Φ_f in CH_2Cl_2, but low Φ_f in H_2O. For example, the Φ_f of **SO_2R2** was determined to be 0.703 in CH_2Cl_2 and 0.09 in H_2O. Their stability in various solutions and photo-stabilities were investigated (Figs. S4–S18 in Supporting information). The *para*-substituted compounds,

* Corresponding author.
E-mail address: zhouxin@qdu.edu.cn (X. Zhou).

https://doi.org/10.1016/j.cclet.2023.108595
1001-8417/

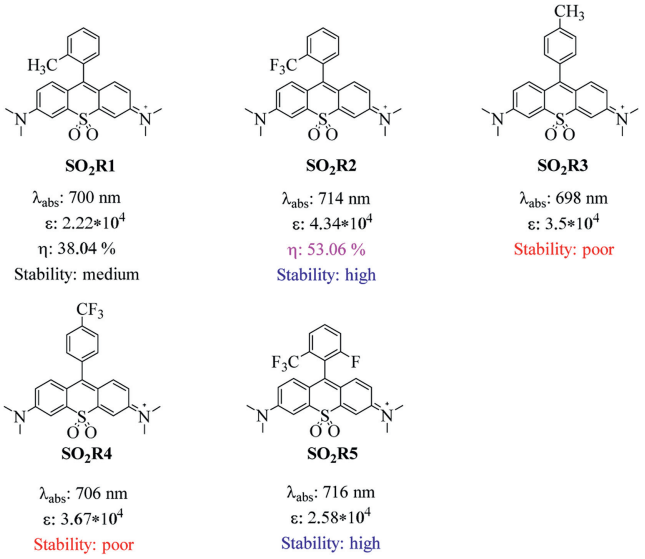

Fig. 1. The chemical structures of **SO_2R1**–**SO_2R5**.

SO_2R3 and **SO_2R4**, showed a dramatic decrease in their absorbance along with a color change from green to colorless and poor photostability. This indicated that nucleophilic attack easily occurred in the presence of most common solvents, such as water, phosphate buffered saline (PBS), methanol, ethanol, isopropanol, *N*,*N*-dimethylformamide (DMF), dimethyl sulfoxide (DMSO), and tetrahydrofuran (THF). On the other hand, *ortho*-substituted compounds displayed considerable stability. **SO_2R1** showed moderate stability, while **SO_2R2** and **SO_2R5** showed high stability and photostability in various solutions. Our findings reveal that the stability of the compound is related to the steric hindrance caused by the substituents. The larger the steric hindrance and more hydrophobic nature of the ortho-substitute, the higher the stability of the dye. We then carried out stability experiments under different pH conditions. As shown in Figs. S2D–F (Supporting information) and Figs. S19–S26 (Supporting information), **SO_2R2** and **SO_2R5** showed high pH tolerance in a broad pH range from 2 to 10 for a long period of time (24 h). This indicates that these compounds have potential for long-term tracking applications without pH influence.

As previously mentioned, both **SO_2R2** and **SO_2R5** showed ideal stability and pH tolerance. Considering the higher absorbance of **SO_2R2** compared to **SO_2R5**, we selected **SO_2R2** for further photothermal transition experiments. When the PBS solution (pH 7.4) of **SO_2R2** was exposed to the light emitting diode (LED) lamp, the temperature increased drastically from 22 °C to 71 °C, as shown in Figs. 2A and B. We investigated the effects of LED lamp power and dye concentration on the photothermal conversion efficiency, as depicted in Figs. 2C and D. After five irradiation/cooling cycles, the compound remained stable, as demonstrated in Figs. 2E and F. Furthermore, we calculated the photothermal conversion efficiency of **SO_2R1** and **SO_2R2** to be 38.04% and 53.06% respectively. We tested the dynamic light scattering (DLS) of **SO_2R2** in water, the data indicated the formation of nanoparticle with a dimeter of 100 nm by self-assembly of **SO_2R2**, as described in Fig. S27 (Supporting information). The nano self-assembly may benefit to higher PTT performance [38].

We evaluated the cytotoxicity of **SO_2R2** to HeLa cells using the cell counting kit-8 (CCK-8) method (Fig. 3B). Results showed that even under dark conditions, the survival rate was over 90%, indicating good cell compatibility and no significant threat to cell viability. To assess the photothermal therapy (PTT) capability of **SO_2R2**, we performed fluorescence microimaging by staining live and dead cells with calcein-AM (AM) and propidium iodide (PI), respectively. Interestingly, the control group for **SO_2R2** showed strong green fluorescence, indicating no apoptosis (Fig. 3A). However, under LED irradiation, almost all HeLa cells in the **SO_2R2** + Laser group emitted a bright red fluorescence signal, indicating that **SO_2R2** displayed efficient PTT effect. Furthermore, additional experiments were performed to determine the dose dependence of HeLa cell survival after 10 min of irradiation with a 730 nm laser (1.0 W/cm^2). The half maximal inhibitory concentration (IC_{50}) of **SO_2R2** was calculated to be 65.82 μmol/L, further highlighting the potency of this compound for PTT.

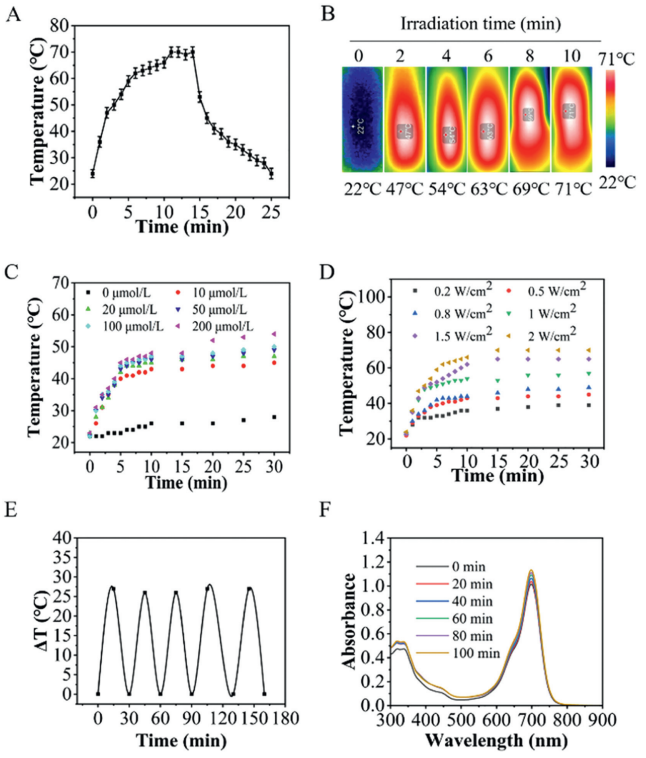

Fig. 2. (A) The temperature change of **SO_2R2** (50 μmol/L) under the irradiation, and the temperature change of natural cooling after 15 min of irradiation (2.0 W/cm^2). (B) The pictures captured by a thermal camera. (C) The concentrations effect of **SO_2R2** under 730–740 nm LED (1.0 W/cm^2). (D) Temperature changes of **SO_2R2** (50 μmol/L) under different powers. (E) The cycles of photothermal heating/cooling for **SO_2R2** (50 μmol/L, 1.0 W/cm^2). (F) Photothermal stability absorption spectra of **SO_2R2** irradiation/cooling in aqueous solution (50 μmol/L, 1.0 W/cm^2).

The strong PA and good biocompatibility of **SO_2R2** make it a promising theragnostic agent. *In vitro* photoacoustic imaging experiments demonstrated a positive correlation between the compound concentration and PA intensity, indicating its potential for high-resolution and high-contrast PA-guided imaging (Fig. 3E). To evaluate the targeting ability of **SO_2R2** *in vivo*, we established a 4T1 tumor-bearing BALB/c mouse model and injected the compound into mice. Photoacoustic imaging revealed a gradual increase in PA intensity at the tumor site, reaching a maximum value after 6 h post-injection, followed by a gradual decrease over time (Figs. 3C and D). The PA values of normal tissue and tumor tissue at different times are shown in the Fig. S28 (Supporting information). These findings demonstrate the potential of **SO_2R2** for non-invasive monitoring of pathological processes in deep tissues.

Subsequently, we conducted anti-tumor studies of **SO_2R2** in nude mice bearing tumors (Fig. 4B). The animal experiments were approved by the Animal Ethical Committee of Medical College of Qingdao University (QDU-AEC-2022040). *In vivo* experiments demonstrated that continuous LED radiation for 10 min caused a

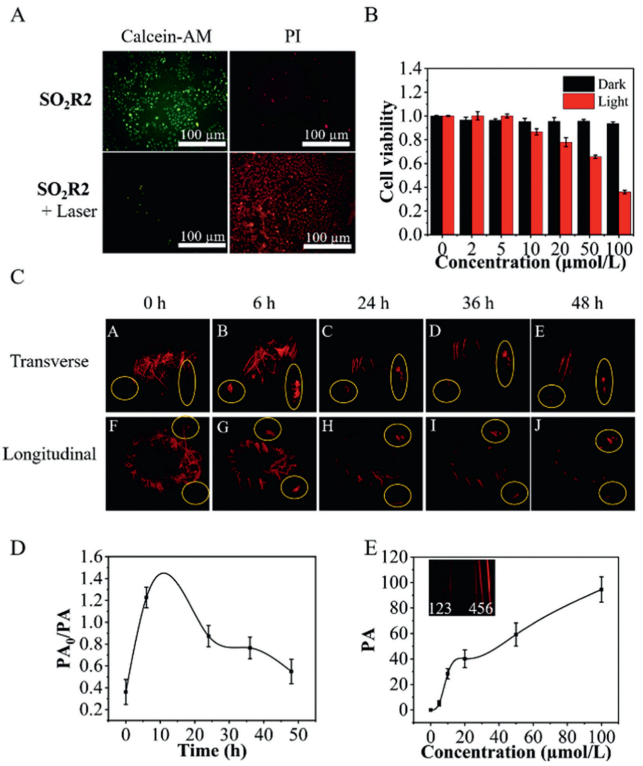

Fig. 3. (A) Fluorescence microscopy imaging of HeLa cells stained with calcein (AM, stained live cells, green color) and pyridine iodide (PI, stained dead cells, red color). Scale bar: 100 μm. (B) Cytotoxicity assays for incubating HeLa cells with and without light for 10 min (1.0 W/cm^2). The data are shown as mean ± standard deviation (SD) ($n = 4$). (C) PA imaging of tumor sites after mice intravenous injection of **SO_2R2** (50 μmol/L). Circles indicate tumors. (D) Photoacoustic signals of PA_0/PA (tumor tissue/normal tissue) at different times. The data are shown as mean ± SD ($n = 3$). (E) *In vitro* PA plot of **SO_2R2** at different concentrations. The data are shown as mean ± SD ($n = 3$).

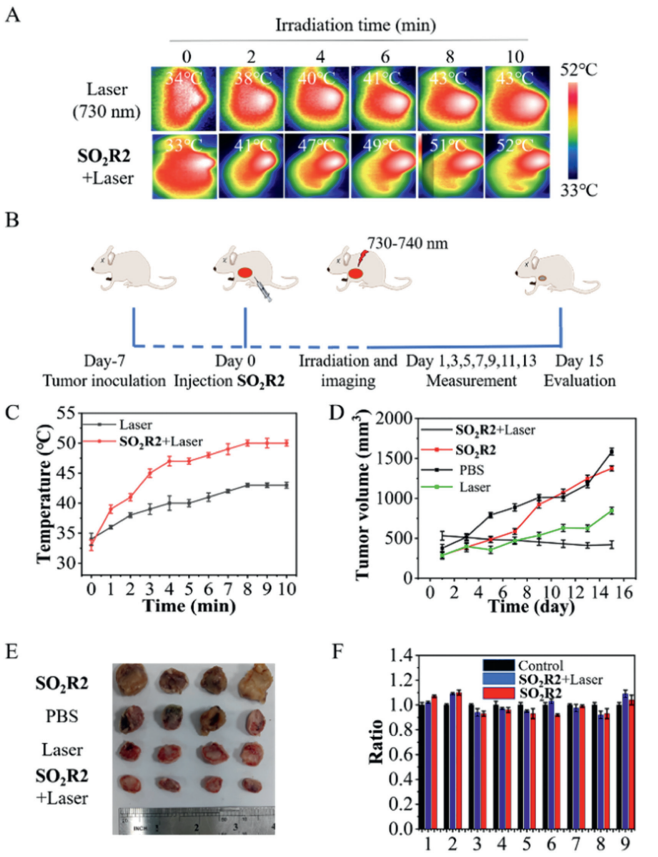

Fig. 4. (A) The tumor area was injected with **SO_2R2** (100 μL, 50 μmol/L) and illuminated with a 730–740 nm LED (1.0 W/cm^2), while the temperature change of the tumor site was recorded in real time with a thermal imager. (B) Schematic diagram of tumor-bearing mice model establishment and treatment operation. (C) Temperature curves of the tumors under 730–740 nm irradiation. The data are shown as mean ± SD ($n = 4$). (D) The tumor volume of the mice in the experimental group and the control group *in vivo* within 15 days. The data are shown as mean ± SD ($n = 4$). (E) Tumor solid plot of dissected mice in experimental *versus* control group. (F) 0.5–1 mL of blood was drawn from mice using bleed removal method for routine blood analysis. 1–9 represent MCHC (mean corpuscular hemoglobin concentration), PLT, HGB (hemoglobin concentration), MCV (mean corpuscular volume), HCT (hematocrit), NEUT (neutrophil), MCH (mean corpuscular hemoglobin), RBC, WBC, respectively. The data are shown as mean ± SD ($n = 4$).

rapid increase in temperature near the solid tumor from 34 °C to 54 °C, while the temperature near the mouse tumor without injecting the photothermal reagent remained relatively unchanged (Figs. 4A and C). Randomly divide all tumor-bearing mice into 4 groups of 3 mice each. The mice were then divided into four groups and subjected to 15 days of photothermal treatment. The results showed that the tumor volume of the **SO_2R2** + laser group was significantly reduced, while the tumor volume of control groups increased significantly. These findings clearly demonstrate the excellent *in vivo* photothermal effect of **SO_2R2**, which effectively kills tumor cells and inhibits tumor growth (Figs. 4D and E, Fig. S29 in Supporting information). These results indicate that **SO_2R2** has great potential for use in cancer therapy. The biosafety evaluation involved monitoring various blood biochemical parameters of mice after 20 days of **SO_2R2** injection [39]. The results showed that all markers in the **SO_2R2** + laser group were similar to those in the control group. Notably, red blood cells (RBC), white blood cells (WBC), and platelets (PLT) were all within the normal range, indicating that **SO_2R2** had negligible long-term *in vivo* toxicity (Fig. 4F). These findings establish **SO_2R2** as a highly promising imaging-assisted PTT agent with minimal systemic toxicity.

In this study, we synthesized five sulfone rhodamines and investigated their substitution effects on stability. The data showed that the *ortho*-substituent is crucial for protecting the 9-site of the rhodamine core, preventing nucleophilic attack. **SO_2R2** demonstrated high stability and strong absorbance at 714 nm. It also showed excellent photothermal conversion efficiency of 53.06% and generated strong PA. The excellent safety profile of **SO_2R2**, coupled with its impressive photothermal effect and *in vivo* targeting ability, make it an ideal candidate for imaging-assisted PTT in the near-infrared window.

Declaration of competing interest

The authors declare that they have no known competing financial interests or personal relationships that could have appeared to influence the work reported in this paper.

Acknowledgments

Prof. Xin Zhou acknowledges the National Natural Science Foundation of China (Nos. 21762045, 21911540466), Shandong Provincial Natural Science Foundation (No. ZR2019YQ12), China Postdoctoral Science Foundation (No. 219M652306), and Taishan Scholar Project (No. tsqn201812049) for supporting this work.

Supplementary material

Supplementary material associated with this article can be found, in the online version, at doi:10.1016/j.cclet.2023.108595.

References

[1] Y. Liu, P. Bhattarai, Z. Dai, X. Chen, Chem. Soc. Rev. 48 (2019) 2053–2108.
[2] X. Zhen, C. Xie, K. Pu, Angew. Chem. Int. Ed. 57 (2018) 3938–3942.
[3] L. Gai, R. Zhang, X. Shi, et al., Chem. Sci. 14 (2023) 1434–1442.
[4] X. Li, E.Y. Park, Y. Kang, et al., Angew. Chem. Int. Ed. 59 (2020) 8630–8634.
[5] Y.W. Chen, Y.L. Su, S.H. Hu, S.Y. Chen, Adv. Drug. Deliv. Rev. 105 (2016) 190–204.
[6] J. Qiao, X.F. Li, L. Qi, Chin. Chem. Lett. 33 (2022) 3193–3196.
[7] K. Li, M. Lu, X.H. Xia, Y.Y. Huang, Chin. Chem. Lett. 32 (2021) 1010–1016.
[8] H. Wang, J.L. Yang, P.H. Cao, et al., Chin. Chem. Lett. 31 (2020) 3015–3026.
[9] Q. Zheng, X. Liu, Y. Zheng, et al., Chem. Soc. Rev. 50 (2021) 5086–5125.
[10] H. Wang, K.F. Xue, Y. Yang, et al., J. Am. Chem. Soc. 144 (2022) 2360–2367.
[11] P. Lin, Y. Xue, X. Mu, et al., Small 18 (2022) e2200179.
[12] X. Mu, Y. Lu, F. Wu, et al., Adv. Mater. 32 (2020) e1906711.
[13] Y. Yan, H. Fu, J. Wang, et al., Chem. Commun. 55 (2019) 10940–10943.
[14] Q. Miao, K. Pu, Adv. Mater. 30 (2018) e1801778.
[15] H.B. Cheng, Y. Li, B.Z. Tang, J. Yoon, Chem. Soc. Rev. 49 (2020) 21–31.
[16] Y.Q. Shi, D.Z. Zhu, D.J. Wang, et al., Coord. Chem. Rev. 471 (2022) 214725.
[17] Q. Cheng, Y. Tian, H. Dang, et al., Adv. Healthc. Mater. 11 (2022) e2101697.
[18] L. Teng, G. Song, Y. Liu, et al., J. Am. Chem. Soc. 141 (2019) 13572–13581.
[19] R. Zhang, Z. Wang, L. Xu, et al., Anal. Chem. 91 (2019) 12476–12483.
[20] Q. Wang, Y.N. Dai, J.Z. Xu, et al., Adv. Funct. 29 (2019) 1901480.
[21] J. Li, W. Zhang, W. Ji, et al., J. Mater. Chem. B 9 (2021) 7909–7926.
[22] J. Huo, Q. Jia, H. Huang, et al., Chem. Soc. Rev. 50 (2021) 8762–8789.
[23] Z.L. Ding, Y.H. Gu, C. Zheng, et al., Coord. Chem. Rev. 464 (2022) 214564.
[24] H.S. Han, K.Y. Choi, Biomedicines 9 (2021) 305.
[25] L.Y. Zhao, Y.M. Liu, R. Chang, R.R. Xing, X.H. Yan, Adv. Funct. 29 (2019) 1806877.
[26] Y. Cao, D. Wei, L. Yang, et al., Adv. Healthc. Mater. 11 (2022) e2102526.
[27] Y. Liu, H. Wang, S. Li, et al., Nat. Commun. 11 (2020) 1724.
[28] P. Gao, H. Wang, Y.Y. Cheng, Chin. Chem. Lett. 33 (2022) 575–586.
[29] Y. Li, M. Wang, F. Wang, S. Lu, X. Chen, Molecules (2023) e20220003.
[30] K. Wang, D. Xi, C. Liu, et al., Chin. Chem. Lett. 31 (2020) 2955–2959.
[31] L. Wang, W. Du, Z. Hu, et al., Angew. Chem. Int. Ed. 58 (2019) 14026–14043.
[32] M. Beija, C.A. Afonso, J.M. Martinho, Chem. Soc. Rev. 38 (2009) 2410–2433.
[33] M. Fu, Y. Xiao, X. Qian, D. Zhao, Y. Xu, Chem. Commun. (2008) 1780–1782.
[34] F. Deng, L. Liu, W. Huang, et al., Spectrochim. Acta A Mol. Biomol. Spectrosc. 240 (2020) 118466.
[35] K.V. Vygranenko, Y.M. Poronik, A. Wrzosek, A. Szewczyk, D.T. Gryko, Chem. Commun. 57 (2021) 7782–7785.
[36] J. Liu, Y.Q. Sun, H. Zhang, et al., ACS Appl. Mater. Interfaces 8 (2016) 22953–22962.
[37] E. Feng, L. Jiao, S. Tang, et al., Chem. Eng. J. 432 (2022) 134355.
[38] E. Feng, Y. Liu, S. Lv, et al., Adv. Funct. 32 (2022) 2209258.
[39] X.L.E. Mu, F.P. Wu, Y. Tang, et al., Aggregate 3 (2022) e170.